Somatic Activating Mutations in *GNAQ* and *GNA11* Are Associated with Congenital Hemangioma

Ugur M. Ayturk,[1,2,9] Javier A. Couto,[3,9] Steven Hann,[1] John B. Mulliken,[3,4] Kaitlin L. Williams,[1] August Yue Huang,[1,2] Steven J. Fishman,[4,5] Theonia K. Boyd,[6] Harry P.W. Kozakewich,[4,6] Joyce Bischoff,[5,7] Arin K. Greene,[3,4] and Matthew L. Warman[1,2,4,8,*]

Congenital hemangioma is a rare vascular tumor that forms in utero. Postnatally, the tumor either involutes quickly (i.e., rapidly involuting congenital hemangioma [RICH]) or partially regresses and stabilizes (i.e., non-involuting congenital hemangioma [NICH]). We hypothesized that congenital hemangiomas arise due to somatic mutation and performed massively parallel mRNA sequencing on affected tissue from eight participants. We identified mutually exclusive, mosaic missense mutations that alter glutamine at amino acid 209 (Glu209) in GNAQ or GNA11 in all tested samples, at variant allele frequencies (VAF) ranging from 3% to 33%. We verified the presence of the mutations in genomic DNA using a combination of molecular inversion probe sequencing (MIP-seq) and digital droplet PCR (ddPCR). The Glu209 GNAQ and GNA11 missense variants we identified are common in uveal melanoma and have been shown to constitutively activate MAPK and/or YAP signaling. When we screened additional archival formalin-fixed paraffin-embedded (FFPE) congenital cutaneous and hepatic hemangiomas, 4/8 had *GNAQ* or *GNA11* Glu209 variants. The same *GNAQ* or *GNA11* mutation is found in both NICH and RICH, so other factors must account for these tumors' different postnatal behaviors.

Congenital hemangiomas are rare vascular tumors that are present at birth. They are different from common infantile hemangiomas that rapidly enlarge postnatally and immunostain for the cell surface marker GLUT1.[1] In contrast, congenital hemangiomas are GLUT1 negative and display one of two clinical patterns: "rapidly involuting congenital hemangioma" (RICH)[2,3] or "non-involuting congenital hemangioma" (NICH).[4] RICH can be detected prenatally (as early as 12 weeks gestation) and presents in a newborn as a raised, gray-violaceous solitary cutaneous tumor with fine telangiectasias, ectatic veins, and a pale halo (Figure 1). RICH demonstrates fast-flow and can be associated with congestive cardiac failure and transient low-grade thrombocytopenia. If there are not overwhelming complications from heart failure or hemorrhagic ulceration, the tumor rapidly regresses by 6–14 months, leaving a patch of subcutaneous atrophy, dilated veins, and persistent fast-flow. RICH is also well documented to occur in the liver (Figure 1), where it spontaneously regresses just as in skin.[5] The second category of congenital hemangioma (NICH) presents as a well-circumscribed, plaque-like tumor with a purple-pink hue, pale rim, coarse telangiectasia, and fast-flow (Figure 1). It remains unchanged throughout childhood; however, there are uncommon examples of growth and expansion in adolescence.[6] In some cases RICH can cease regressing and transform into NICH.[7,8] There are histopathological similarities between RICH and NICH (Figure 1) and between congenital hemangioma and placental chorangioma, suggesting that chorangioma might be the placental counterpart of cutaneous and intrahepatic congenital hemangioma.[9]

We hypothesized that somatic mutations initiate the formation of congenital hemangiomas and searched for these mutations by performing massively parallel sequencing on fresh frozen specimens.

The Committee on Clinical Investigation of Boston Children's Hospital approved this study. Congenital hemangioma samples were collected during a clinically indicated procedure, and all participants provided written consent. Tissues were immediately flash-frozen or placed in RNAlater (Thermo Fisher Scientific) and stored at −80°C until further processing. The original intent was to perform RNA-seq looking for coding sequence mutations or genetic alterations that might produce chimeric or miss-spliced transcripts and to perform whole-exome sequencing (WES) looking for coding sequence mutations in genes that were not highly expressed in affected tissue. RNA-seq libraries were prepared via standard Illumina TruSeq protocols and sequenced on one flowcell of an Illumina HiSeq 2500 system. We did not perform WES because we were able to successfully identify mutations with RNA-seq.

We generated 32–47 million 100-bp paired-end reads per RNA-seq library. Following the Genome Analysis Toolkit (GATK) best practices workflow,[10] we mapped each set of reads to the reference human genome (GRCh37) with STAR aligner,[11] removed PCR duplicates with Picard, realigned the reads around small insertions and deletions, and recalibrated the base quality scores with GATK.[12] We

[1]Department of Orthopaedic Surgery, Boston Children's Hospital, Boston, MA 02115, USA; [2]Department of Genetics, Harvard Medical School, Boston, MA 02115, USA; [3]Department of Plastic and Oral Surgery, Boston Children's Hospital, Boston, MA 02115, USA; [4]Vascular Anomalies Center, Boston Children's Hospital, Boston, MA 02115, USA; [5]Department of Surgery, Boston Children's Hospital, Boston, MA 02115, USA; [6]Department of Pathology, Boston Children's Hospital, Boston, MA 02115, USA; [7]Vascular Biology Program, Boston Children's Hospital, Boston, MA 02115, USA; [8]Howard Hughes Medical Institute, Boston Children's Hospital, Boston, MA 02115, USA
[9]These authors contributed equally to this work
*Correspondence: matthew.warman@childrens.harvard.edu
http://dx.doi.org/10.1016/j.ajhg.2016.03.009.

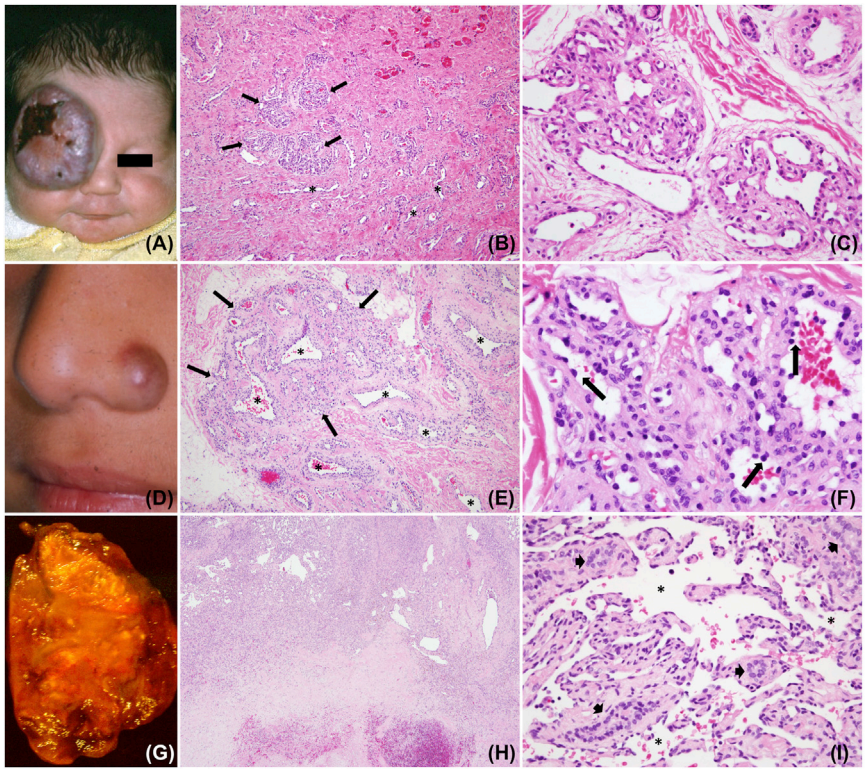

Figure 1. Representative Gross and Histological Images of RICH, NICH, and Solitary Congenital Hepatic Hemangioma from Three Participants

Shown are RICH (A–C), NICH (D–F), and solitary congenital hepatic hemangioma (G–I).

(A) Supraorbital purple tumor with central depression and ulceration in a 1-week-old infant (participant 8 with RICH).

(B) Hematoxylin and eosin (H&E) staining of the affected tissue imaged at 100× reveals small lobules (arrows) surrounded by abundant dense fibrous tissue where lobules have involuted and only draining channels remain (asterisks).

(C) H&E staining at 400× reveals lobular capillaries containing enlarged lumens and minimally prominent endothelium.

(D) Raised erythematous nodule at the left nasal ala in a 5-year-old child (participant 4 with NICH).

(E) H&E staining at 100× reveals a large lobule (arrows) with prominent intra- and peri-lobular channels (asterisks).

(F) H&E staining at 600× shows a hobnailed endothelium (arrows) lining lobular channels surrounded by fibrous tissue.

(G) Excised 5 cm hepatic mass with pallor, extensive infarction, focal calcification, and hemorrhage in a 3-month-old infant (participant 16 with hepatic RICH).

(H) H&E staining at 20× reveals a highly vascular rim superiorly and an acellular infarcted and hemorrhagic zone inferiorly.

(I) H&E staining at 400× shows a minimally prominent endothelium lining widened hepatic sinusoids (asterisks) with cords containing a few bile ducts (arrowheads) but devoid of hepatocytes.

then compiled single-nucleotide variant lists with Samtools[13] and identified positions with a minimum of 20× read depth, 3× variant read depth, and 10% variant allele frequency using VarScan.[14] We removed variants with greater than 40% variant allele frequency, assuming that these changes most likely represent germline variants rather than somatic changes. We further filtered the variants by removing those previously reported in the Exome Variant Server (ESP6500), 1000 Genomes Project, Exome Aggregation Consortium (v.0.3), and dbSNP as a non-clinical entry (build 138). We annotated the remaining variants with ANNOVAR.[15]

A total of 43 genes exhibited protein sequence altering variants in ≥3 of 8 specimens (Figure S1). We narrowed this list further by comparing these variants to those found in RNA-seq data from unrelated vascular lesions (arteriovenous malformation [n = 3] and common infantile hemangioma [n = 1]). A total of 12 genes contained a variant found

Table 1. Variant Filtering Strategy Employed in the Analysis of RNA-Seq Data

Participant	1	2	3	4	5	6	7	8	Average
Min 20× read depth, 3× var read depth, 10% var allele freq	56,331	49,047	40,440	38,348	37,672	32,473	39,380	26,900	40,074
Known variants filtered	24,333	18,454	12,671	12,893	11,756	10,206	11,236	9,570	13,890
Coding sequence variants	279	208	234	253	241	276	261	348	263
Nonsynonymous variants	172	120	144	138	134	155	164	221	156
Variants without strand bias	133	83	94	105	99	114	110	167	113
Variants with <40% allele freq	93	62	57	92	70	92	87	139	87
Genes with variants in ≥3 samples, not in negative controls	*ATN1, B3GNT2, GNAQ, IL13RA1, NBPF11, PLEKHO1, SMC4, SSC5D, TBX3, TCF7L2, TCHP, POLR2J2/UPK3BL*								12

Table 2. Participants Screened for *GNAQ* and *GNA11* Variants

Participant	Phenotype	Age	Sex	Location	Source	Variant	RNA	DNA (MIP-seq)	DNA (ddPCR)	Control DNA (ddPCR)
1	NICH	8 years	male	chest	frozen tissue	GNAQ pGlu209Leu (c.626A>T)	2/6 (33%)	–	101/1,853 (5%)	0/1,499 (0%)
2	NICH	9 years	male	neck	frozen tissue	GNAQ pGlu209Pro (c.626A>C)	1/10 (10%)	–	392/6,061 (6%)	0/2,215 (0%)
3	NICH	14 years	female	temple	frozen tissue	GNA11 pGlu209Leu (c.626A>T)	15/124 (12%)	13/211 (6%)	84/1,042 (8%)	0/2,498 (0%)
4	NICH	5 years	male	nose	frozen tissue	GNAQ pGlu209Leu (c.626A>T)	3/15 (20%)	–	235/3,233 (7%)	0/2,359 (0%)
5	NICH	7 years	male	nose	frozen tissue	GNAQ pGlu209Leu (c.626A>T)	7/51 (14%)	–	61/759 (8%)	–
6	NICH	2.5 years	male	neck	frozen tissue	GNA11 pGlu209Leu (c.626A>T)	3/103 (3%)	–	15/633 (2%)	–
7	RICH	3 years	male	lower extremity	frozen tissue	GNAQ pGlu209His (c.627A>C)	7/30 (23%)	–	–	–
8	RICH	1 week	male	orbital area	frozen tissue	GNAQ pGlu209Leu (c.626A>T)	6/31 (19%)	–	–	–
9	NICH	12 years	male	lower extremity	FFPE tissue	GNAQ pGlu209Pro (c.626A>C)	–	1139/19,657 (6%)	125/1,089 (11%)	–
10	NICH	14 months	male	lower extremity	FFPE tissue	NA	–	3/1,383 (< 1%)	0/640 (0%)	–
11	RICH	3 months	male	lower extremity	FFPE tissue	GNAQ pGlu209Leu (c.626A>T)	–	-	26/717 (4%)	–
12	NICH	3 years	male	ear	FFPE tissue	NA	–	1/400 (< 1%)	-	–
13	RICH	2 weeks	female	upper extremity	FFPE tissue	NA	–	2/772 (< 1%)	0/516 (0%)	–
14	NICH	2 years	male	lower extremity	FFPE tissue	NA	–	2/179 (1%)	0/152 (0%)	–
15	RICH	2 weeks	male	lower extremity	FFPE tissue	GNA11 pGlu209Leu (c.626A>T)	–	–	27/2,576 (1%)	–
16	RICH	4 months	male	liver	FFPE tissue	GNA11 pGlu209Leu (c.626A>T)	–	–	52/537 (10%)	–
17	CHOR	neonatal	female	placenta	FFPE tissue	NA	–	0/850 (0%)	–	–
18	CHOR	neonatal	female	placenta	FFPE tissue	NA	–	3/1,855 (< 1%)	–	–
19	CHOR	neonatal	female	placenta	FFPE tissue	NA	–	3/1,875 (< 1%)	–	–
20	CHOR	neonatal	female	placenta	FFPE tissue	NA	–	7/2,233 (< 1%)	–	–

RNA and DNA (MIP-seq) columns indicate read depth, and DNA (ddPCR) column indicates number of droplets. The rate of variant/total alleles is also depicted in the aforementioned columns. For samples that were not associated with a mutation (indicated with NA), available MIP-seq and ddPCR results with the lowest power (in terms of read depth and number of droplets) are depicted. Control DNA samples were retrieved from blood or saliva. Abbreviations are as follows: NICH, non-involuting congenital hemangioma; RICH, rapidly involuting congential hemangioma; CHOR, chorangioma. Dash (–) indicates that the assay was not performed.

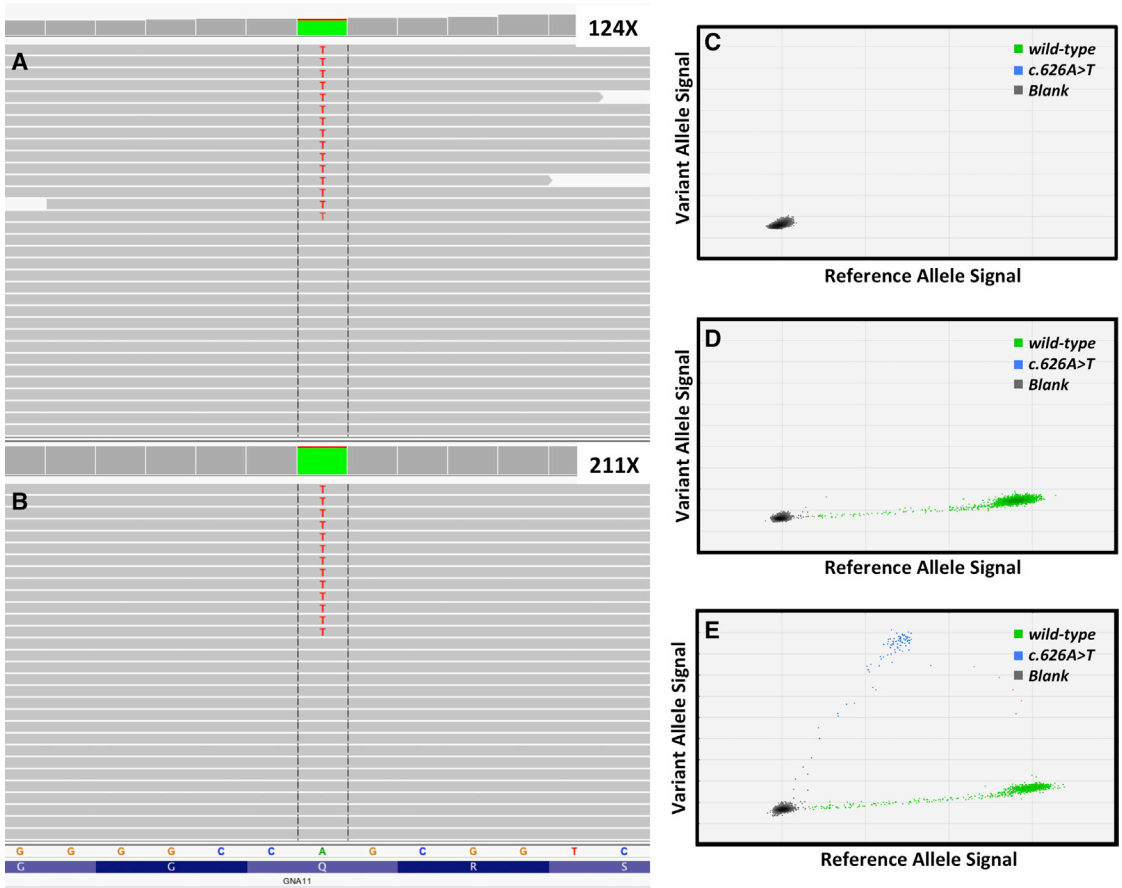

Figure 2. Detection of the *GNA11* c.626A>T (p.Glu209Leu) Allele in Congenital Hemangioma Specimen from Participant 3 with NICH
(A) IGV screenshot indicating 12% variant allele frequency in *GNA11* transcripts measured by RNA-seq. 124× indicates the depth of coverage at position 626.
(B) IGV screenshot indicating 6% variant allele frequency in *GNA11* measured by MIP-seq. 211× indicates the depth of coverage at position 626.
(C) Water-negative control for the ddPCR assay shows no flourescence for *GNA11* wild-type or variant alleles.
(D) ddPCR results of human DNA from unaffected control tissue indicates the presence of only the *GNA11* wild-type allele.
(E) ddPCR results of congenital hemangioma indicates the presence of wild-type and variant (8%) alleles.

only in the congenital hemangioma samples (Table 1). The variants found in the other RNA-seq datasets were assumed to be associated with RNA editing or with errors in sequencing, mapping, or annotation. Close inspection of variants in the 12 remaining genes for potential mismapping, sequencing errors, and lack of evolutionary conservation left only variants in *GNAQ* (MIM: 600998) as likely true-positive somatic mutations (Tables 2 and S1). *GNAQ* encodes guanine nucleotide binding protein G(q) alpha, a subunit within a complex that hydrolyzes the intracellular messenger GTP to GDP. GNAQ shares 90% protein sequence similarity with GNA11 (MIM: 139313). Somatic missense mutations that alter codon 209 in GNAQ (GenBank: NP_002063.2) and GNA11 (GenBank: NP_002058.2) have been reported in >80% of uveal melanomas.[16,17] A different somatic mutation in *GNAQ* (GRCh37; GenBank: NM_002072.4, NP_002063.2; c.548G>A [p.Arg183Gln]) occurs in isolated capillary malformations and in individuals with Sturge-Weber syndrome (MIM: 185300).[18] Stringent filtering revealed evidence for a *GNAQ* missense mutation in three of eight samples (Figure S1). When we reanalyzed with less stringent filtering, we found that six of eight samples had a somatic *GNAQ* mutation and the remaining two samples had a somatic *GNA11* mutation (Table 2).

We confirmed that the mutations were real by testing DNA from six of eight samples via an orthologous method, digital droplet PCR (ddPCR), and/or molecular inversion probe sequencing (MIP-seq) (Table 2 and Figure 2). We performed ddPCR (Table S2) as previously described[19] and considered variants present at frequencies ≥ 1% to represent true positives. We also verified that the mutations we identified are somatic by testing control DNA (extracted from blood or saliva) of four participants via ddPCR (Table 2). For MIP-seq, we enriched the genomic DNA samples for the protein-coding sequences of *GNAQ* and *GNA11* by hybridization to probes (Table S3) containing an 8-nucleotide barcode that uniquely identifies individual MIPs. MIP capture and sequencing were performed as previously described.[20] Raw reads were mapped to the reference

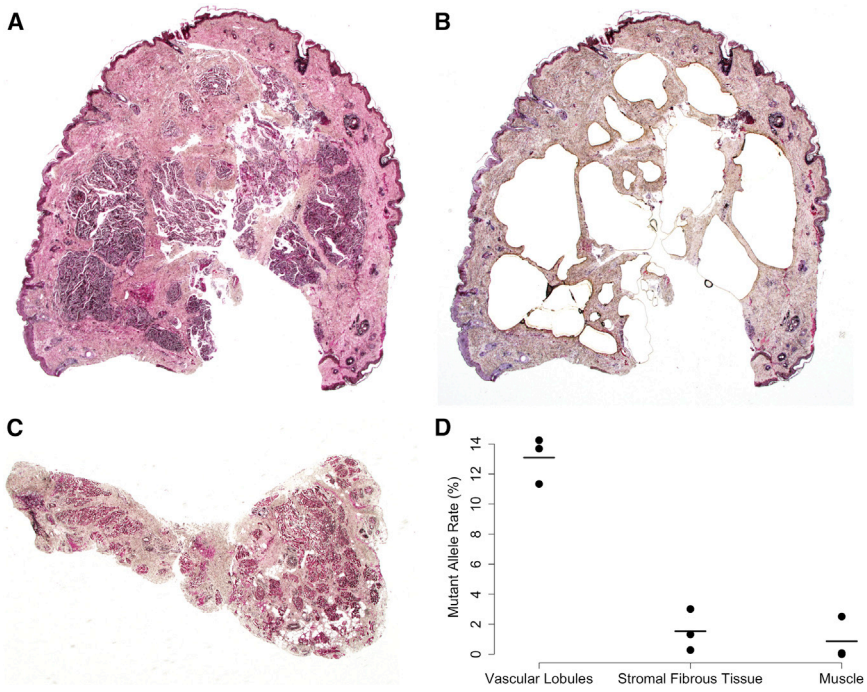

Figure 3. Mutant Allele Frequency in Capillary-Enriched Lobules Is Higher than That in the Surrounding Stromal Tissue within Congenital Hemangioma

(A) Pre-laser capture image of NICH showing multiple dermal vascular lobules from participant 4 (staining dark blue in hematoxylin and eosin-stained section, ×20 magnification).

(B) Post-laser capture image of the section depicted in (A) showing absence of virtually all vascular lobules (hematoxylin and eosin-stained section, ×20 magnification).

(C) Pre-laser capture of skeletal muscle, fibrous tissue, and fat uninvolved tissue by the NICH shown in (A) and (B) (hematoxylin and eosin-stained section, ×20 magnification) that was resected en bloc.

(D) Graph depicting the *GNAQ* c.626A>T allele frequencies in DNA extracted from the capillary enriched lobules (A), the residual tissue (B), and the adjacent muscle tissue (C) measured in triplicate by ddPCR (dots). Solid lines indicate the average of the three measurements.

human genome sequence (GRCh37) with BWA; PCR duplicates were removed with FastqMcf and Picard. The minimum read depths for *GNAQ* c.626A>T and *GNA11* c.626A>T (GRCh37, GenBank: NM_002067.4) were 2,032× and 179×, respectively. We considered true positive somatic variants to have allele frequencies >2%. Using a combination of the aforementioned ddPCR and MIP-seq assays, we also analyzed eight archival formalin-fixed paraffin-embedded (FFPE) congenital hemangiomas and four chorangioma samples. Four of the hemangiomas contained a likely somatic *GNAQ* or *GNA11* mutation, whereas no such mutations were found in the chorangiomas (Table 2).

Our findings expand the spectrum of genes and alleles that are somatically altered in congenital vascular anomalies (Figure S2).[18–29] Of interest is that the same mutation (i.e., *GNAQ* c.626A>T and *GNA11* c.626A>T) occurs in RICH and NICH, implying that other genetic, epigenetic, and/or environmental factors probably influence these lesions' postnatal behavior. Because *GNAQ* and *GNA11* mutations are common in highly metastatic uveal melanomas,[16,17] identifying factors that determine the postnatal behavior of RICH and NICH might suggest new strategies for treating uveal melanoma. Thus far, we observed mutations affecting Glu209 in GNAQ or GNA11 only in congenital hemangioma, whereas we and other investigators[18,30,31] have identified mutations affecting Arg183 only in capillary malformations. Our data indicate that, with respect to congenital hemangiomas, GNAQ and GNA11 have functional overlap. Consistent with functional overlap in nonmalignant conditions, somatic mutations affecting either codon 183 or 209 in GNAQ and GNA11 have also been found in phakomatosis pigmentovascularis and extensive dermal melanocytosis.[32] However, a role for GNA11 that does not overlap with that of GNAQ can be inferred from recent studies of inherited hypocalcemia and hypercalcemia caused by mutations in GNA11 but not GNAQ.[33–36] In vitro studies indicated that missense mutations altering Arg183 and Glu209 both activate GTP-dependent signaling, but might do so via different pathways and with different efficiency.[18,37,38] Therefore, it is critical to understand the cell-type-specific, context-specific, and allele-specific effects of somatic *GNAQ* or *GNA11* mutations during vasculogenesis. For example, the *GNAQ* c.548G>A (p.Arg183Gln) mutation in sporadic capillary malformations was shown to be enriched in endothelial cells that line blood vessels,[30] whereas in lymphatic malformations activating *PIK3CA* (MIM: 171834), mutations were present in the lymphatic endothelial cells.[39,40,41] To determine which features within a congenital hemangioma sample are enriched for mutant cells, we performed laser capture microdissection on a FFPE tissue section from participant 4. We observed a mutant allele frequency of 13% in the vascular-enriched lobules within the lesion, whereas the remaining tissues exhibit less than 2% mutant allele frequency (Figure 3).

We were unable to identify strongly suggestive *GNAQ* or *GNA11* mutations in 4/16 congenital hemangiomas, leading us to conclude that the frequency of mutated cells in some specimens was either below our threshold of detection or that congenital hemangiomas exhibit further locus heterogeneity. Although our sample size for chorangiomas is small, our data indicate that chorangioma is probably not the placental counterpart of congenital hemangiomas associated with mutations altering Glu209 in GNAQ or GNA11.

In contrast to an earlier study in which we detected somatic mutations in *PIK3CA* with WES but not with RNA-seq,[23] RNA-seq was useful in this study. For WES, the sensitivity of detecting somatic mutations is dependent on depth of coverage and frequency of mutant cells (Figure S3). Interestingly, when we compared the relative frequencies of the *GNAQ* and *GNA11* mutant allele at the RNA and DNA levels in the affected tissue specimens for which we had paired RNA and DNA, the mutant allele frequency was always higher in the RNA (Table 2). This latter finding is compatible with mutation-containing cells within the affected tissue expressing *GNAQ* or *GNA11* at a greater level relative to other cells. Thus, in addition to the advantages of using RNA-seq to find mutations that produce abnormal splicing or chimeric transcripts, RNA-seq can be advantageous for detecting somatic coding sequence mutations.

Supplemental Data

Supplemental Data include three figures and three tables and can be found with this article online at http://dx.doi.org/10.1016/j.ajhg.2016.03.009.

Acknowledgments

We are grateful for the contributions of the participants to this study. This work was supported by NIH grants R01-AR064231 (to M.L.W.), R01-HL096384 (to J.B.), and R21-HD081004 (to A.K.G.).

Received: December 21, 2015
Accepted: March 14, 2016
Published: April 7, 2016

Web Resources

The URLs for data presented herein are as follows:

1000 Genomes, http://browser.1000genomes.org
ANNOVAR, http://annovar.openbioinformatics.org/en/latest/
Burrows-Wheeler Aligner, http://bio-bwa.sourceforge.net/
dbSNP, build 138, http://www.ncbi.nlm.nih.gov/projects/SNP/
ExAC Browser, http://exac.broadinstitute.org/
Fastq-MCF, https://code.google.com/p/ea-utils/wiki/FastqMcf
GATK, https://www.broadinstitute.org/gatk/
NHLBI Exome Sequencing Project (ESP) Exome Variant Server, http://evs.gs.washington.edu/EVS/
OMIM, http://www.omim.org/
Picard, http://broadinstitute.github.io/picard/
RefSeq, http://www.ncbi.nlm.nih.gov/RefSeq
samtools, https://github.com/samtools/
STAR Aligner, https://github.com/alexdobin/STAR/releases
VarScan, http://varscan.sourceforge.net/

References

1. North, P.E., Waner, M., Mizeracki, A., and Mihm, M.C., Jr. (2000). GLUT1: a newly discovered immunohistochemical marker for juvenile hemangiomas. Hum. Pathol. *31*, 11–22.
2. Berenguer, B., Mulliken, J.B., Enjolras, O., Boon, L.M., Wassef, M., Josset, P., Burrows, P.E., Perez-Atayde, A.R., and Kozakewich, H.P. (2003). Rapidly involuting congenital hemangioma: clinical and histopathologic features. Pediatr. Dev. Pathol. *6*, 495–510.
3. Boon, L.M., Enjolras, O., and Mulliken, J.B. (1996). Congenital hemangioma: evidence of accelerated involution. J. Pediatr. *128*, 329–335.
4. Enjolras, O., Mulliken, J.B., Boon, L.M., Wassef, M., Kozakewich, H.P., and Burrows, P.E. (2001). Noninvoluting congenital hemangioma: a rare cutaneous vascular anomaly. Plast. Reconstr. Surg. *107*, 1647–1654.
5. Fishman, S.J., and Burrows, P.E. (2013). Treatment of visceral vascular tumors. In Mulliken and Young's Vascular Anomalies: Hemangiomas and Malformations, J.B. Mulliken, P.E. Burrows, and S.J. Fishman, eds. (Oxford University Press), pp. 242–245.
6. Mulliken, J.B. (2013). Diagnosis and natural history of hemangiomas. In Mulliken and Young's Vascular Anomalies: Hemangiomas and Malformations, J.B. Mulliken, P.E. Burrows, and S.J. Fishman, eds. (Oxford University Press), pp. 69–110.
7. Mulliken, J.B., and Enjolras, O. (2004). Congenital hemangiomas and infantile hemangioma: missing links. J. Am. Acad. Dermatol. *50*, 875–882.
8. Nasseri, E., Piram, M., McCuaig, C.C., Kokta, V., Dubois, J., and Powell, J. (2014). Partially involuting congenital hemangiomas: a report of 8 cases and review of the literature. J. Am. Acad. Dermatol. *70*, 75–79.
9. Mulliken, J.B., Bischoff, J., and Kozakewich, H.P. (2007). Multifocal rapidly involuting congenital hemangioma: a link to chorangioma. Am. J. Med. Genet. A. *143A*, 3038–3046.
10. Van der Auwera, G.A., Carneiro, M.O., Hartl, C., Poplin, R., Del Angel, G., Levy-Moonshine, A., Jordan, T., Shakir, K., Roazen, D., Thibault, J., et al. (2013). From FastQ data to high confidence variant calls: the Genome Analysis Toolkit best practices pipeline. Curr. Protoc. Bioinformatics *11*, 1, 33.
11. Dobin, A., Davis, C.A., Schlesinger, F., Drenkow, J., Zaleski, C., Jha, S., Batut, P., Chaisson, M., and Gingeras, T.R. (2013). STAR: ultrafast universal RNA-seq aligner. Bioinformatics *29*, 15–21.
12. McKenna, A., Hanna, M., Banks, E., Sivachenko, A., Cibulskis, K., Kernytsky, A., Garimella, K., Altshuler, D., Gabriel, S., Daly, M., and DePristo, M.A. (2010). The Genome Analysis Toolkit: a MapReduce framework for analyzing next-generation DNA sequencing data. Genome Res. *20*, 1297–1303.
13. Li, H., Handsaker, B., Wysoker, A., Fennell, T., Ruan, J., Homer, N., Marth, G., Abecasis, G., and Durbin, R.; 1000 Genome Project Data Processing Subgroup (2009). The Sequence Alignment/Map format and SAMtools. Bioinformatics *25*, 2078–2079.
14. Koboldt, D.C., Zhang, Q., Larson, D.E., Shen, D., McLellan, M.D., Lin, L., Miller, C.A., Mardis, E.R., Ding, L., and Wilson, R.K. (2012). VarScan 2: somatic mutation and copy number alteration discovery in cancer by exome sequencing. Genome Res. *22*, 568–576.
15. Wang, K., Li, M., and Hakonarson, H. (2010). ANNOVAR: functional annotation of genetic variants from high-throughput sequencing data. Nucleic Acids Res. *38*, e164.
16. Van Raamsdonk, C.D., Bezrookove, V., Green, G., Bauer, J., Gaugler, L., O'Brien, J.M., Simpson, E.M., Barsh, G.S., and Bastian, B.C. (2009). Frequent somatic mutations of GNAQ in uveal melanoma and blue naevi. Nature *457*, 599–602.
17. Van Raamsdonk, C.D., Griewank, K.G., Crosby, M.B., Garrido, M.C., Vemula, S., Wiesner, T., Obenauf, A.C., Wackernagel,

W., Green, G., Bouvier, N., et al. (2010). Mutations in GNA11 in uveal melanoma. N. Engl. J. Med. *363*, 2191–2199.
18. Shirley, M.D., Tang, H., Gallione, C.J., Baugher, J.D., Frelin, L.P., Cohen, B., North, P.E., Marchuk, D.A., Comi, A.M., and Pevsner, J. (2013). Sturge-Weber syndrome and port-wine stains caused by somatic mutation in GNAQ. N. Engl. J. Med. *368*, 1971–1979.
19. Couto, J.A., Vivero, M.P., Kozakewich, H.P., Taghinia, A.H., Mulliken, J.B., Warman, M.L., and Greene, A.K. (2015). A somatic MAP3K3 mutation is associated with verrucous venous malformation. Am. J. Hum. Genet. *96*, 480–486.
20. Luks, V.L., Kamitaki, N., Vivero, M.P., Uller, W., Rab, R., Bovée, J.V., Rialon, K.L., Guevara, C.J., Alomari, A.I., Greene, A.K., et al. (2015). Lymphatic and other vascular malformative/overgrowth disorders are caused by somatic mutations in PIK3CA. J. Pediatr. *166*, 1048–54.e1, 5.
21. Eerola, I., Boon, L.M., Mulliken, J.B., Burrows, P.E., Dompmartin, A., Watanabe, S., Vanwijck, R., and Vikkula, M. (2003). Capillary malformation-arteriovenous malformation, a new clinical and genetic disorder caused by RASA1 mutations. Am. J. Hum. Genet. *73*, 1240–1249.
22. Groesser, L., Peterhof, E., Evert, M., Landthaler, M., Berneburg, M., and Hafner, C. (2016). BRAF and RAS mutations in sporadic and secondary pyogenic granuloma. J. Invest. Dermatol. *136*, 481–486.
23. Kurek, K.C., Luks, V.L., Ayturk, U.M., Alomari, A.I., Fishman, S.J., Spencer, S.A., Mulliken, J.B., Bowen, M.E., Yamamoto, G.L., Kozakewich, H.P., and Warman, M.L. (2012). Somatic mosaic activating mutations in PIK3CA cause CLOVES syndrome. Am. J. Hum. Genet. *90*, 1108–1115.
24. Liaw, D., Marsh, D.J., Li, J., Dahia, P.L., Wang, S.I., Zheng, Z., Bose, S., Call, K.M., Tsou, H.C., Peacocke, M., et al. (1997). Germline mutations of the PTEN gene in Cowden disease, an inherited breast and thyroid cancer syndrome. Nat. Genet. *16*, 64–67.
25. Lim, Y.H., Douglas, S.R., Ko, C.J., Antaya, R.J., McNiff, J.M., Zhou, J., Choate, K.A., and Narayan, D. (2015). Somatic activating RAS mutations cause vascular tumors including pyogenic granuloma. J. Invest. Dermatol. *135*, 1698–1700.
26. Limaye, N., Kangas, J., Mendola, A., Godfraind, C., Schlögel, M.J., Helaers, R., Eklund, L., Boon, L.M., and Vikkula, M. (2015). Somatic activating PIK3CA mutations cause venous malformation. Am. J. Hum. Genet. *97*, 914–921.
27. Lindhurst, M.J., Sapp, J.C., Teer, J.K., Johnston, J.J., Finn, E.M., Peters, K., Turner, J., Cannons, J.L., Bick, D., Blakemore, L., et al. (2011). A mosaic activating mutation in AKT1 associated with the Proteus syndrome. N. Engl. J. Med. *365*, 611–619.
28. Vikkula, M., Boon, L.M., Carraway, K.L., 3rd, Calvert, J.T., Diamonti, A.J., Goumnerov, B., Pasyk, K.A., Marchuk, D.A., Warman, M.L., Cantley, L.C., et al. (1996). Vascular dysmorphogenesis caused by an activating mutation in the receptor tyrosine kinase TIE2. Cell *87*, 1181–1190.
29. Rivière, J.B., Mirzaa, G.M., O'Roak, B.J., Beddaoui, M., Alcantara, D., Conway, R.L., St-Onge, J., Schwartzentruber, J.A., Gripp, K.W., Nikkel, S.M., et al.; Finding of Rare Disease Genes (FORGE) Canada Consortium (2012). De novo germline and postzygotic mutations in AKT3, PIK3R2 and PIK3CA cause a spectrum of related megalencephaly syndromes. Nat. Genet. *44*, 934–940.
30. Couto, J.A., Huang, L., Vivero, M.P., Kamitaki, N., Maclellan, R.A., Mulliken, J.B., Bischoff, J., Warman, M.L., and Greene, A.K. (2016). Endothelial cells from capillary malformations are enriched for somatic GNAQ mutations. Plast. Reconstr. Surg. *137*, 77e–82e.
31. Nakashima, M., Miyajima, M., Sugano, H., Iimura, Y., Kato, M., Tsurusaki, Y., Miyake, N., Saitsu, H., Arai, H., and Matsumoto, N. (2014). The somatic GNAQ mutation c.548G>A (p.R183Q) is consistently found in Sturge-Weber syndrome. J. Hum. Genet. *59*, 691–693.
32. Thomas, A.C., Zeng, Z., Rivière, J.B., O'Shaughnessy, R., Al-Olabi, L., St-Onge, J., Atherton, D.J., Aubert, H., Bagazgoitia, L., Barbarot, S., et al. (2016). Mosaic activating mutations in GNA11 and GNAQ are associated with phakomatosis pigmentovascularis and extensive dermal melanocytosis. J. Invest. Dermatol. Published online January 14, 2016. S0022-202X(16)00332-8.
33. Piret, S.E., Gorvin, C.M., Pagnamenta, A.T., Howles, S.A., Cranston, T., Rust, N., Nesbit, M.A., Glaser, B., Taylor, J.C., Buchs, A.E., et al. (2016). Identification of a G-protein subunit-α11 gain-of-function mutation, Val340Met, in a family with autosomal dominant hypocalcemia type 2 (ADH2). J. Bone Miner. Res. Published online January 28, 2016. http://dx.doi.org/10.1002/jbmr.2797.
34. Gorvin, C.M., Cranston, T., Hannan, F.M., Rust, N., Qureshi, A., Nesbit, M.A., and Thakker, R.V. (2016). G-protein subunit-α11 loss-of-function mutation, Thr54Met, causing familial hypocalciuric hypercalcemia type 2 (FHH2). J. Bone Miner. Res. Published online January 5, 2016. http://dx.doi.org/10.1002/jbmr.2778.
35. Nesbit, M.A., Hannan, F.M., Howles, S.A., Babinsky, V.N., Head, R.A., Cranston, T., Rust, N., Hobbs, M.R., Heath, H., 3rd, and Thakker, R.V. (2013). Mutations affecting G-protein subunit α11 in hypercalcemia and hypocalcemia. N. Engl. J. Med. *368*, 2476–2486.
36. Mannstadt, M., Harris, M., Bravenboer, B., Chitturi, S., Dreijerink, K.M., Lambright, D.G., Lim, E.T., Daly, M.J., Gabriel, S., and Jüppner, H. (2013). Germline mutations affecting Gα11 in hypoparathyroidism. N. Engl. J. Med. *368*, 2532–2534.
37. Feng, X., Degese, M.S., Iglesias-Bartolome, R., Vaque, J.P., Molinolo, A.A., Rodrigues, M., Zaidi, M.R., Ksander, B.R., Merlino, G., Sodhi, A., et al. (2014). Hippo-independent activation of YAP by the GNAQ uveal melanoma oncogene through a trio-regulated rho GTPase signaling circuitry. Cancer Cell *25*, 831–845.
38. Yu, F.X., Luo, J., Mo, J.S., Liu, G., Kim, Y.C., Meng, Z., Zhao, L., Peyman, G., Ouyang, H., Jiang, W., et al. (2014). Mutant Gq/11 promote uveal melanoma tumorigenesis by activating YAP. Cancer Cell *25*, 822–830.
39. Couto, J.A., Vivero, M.P., Upton, J., Padwa, B.L., Warman, M.L., Mulliken, J.B., and Greene, A.K. (2015). Facial infiltrating lipomatosis contains somatic PIK3CA mutations in multiple tissues. Plast. Reconstr. Surg. *136* (4, Suppl), 72–73.
40. Boscolo, E., Coma, S., Luks, V.L., Greene, A.K., Klagsbrun, M., Warman, M.L., and Bischoff, J. (2015). AKT hyper-phosphorylation associated with PI3K mutations in lymphatic endothelial cells from a patient with lymphatic malformation. Angiogenesis *18*, 151–162.
41. Osborn, A.J., Dickie, P., Neilson, D.E., Glaser, K., Lynch, K.A., Gupta, A., and Dickie, B.H. (2015). Activating PIK3CA alleles and lymphangiogenic phenotype of lymphatic endothelial cells isolated from lymphatic malformations. Hum. Mol. Genet. *24*, 926–938.